Computationally Assisted Design of Polarizing Agents for Dynamic Nuclear Polarization Enhanced NMR: The AsymPol Family

Frédéric Mentink-Vigier,[†,‖] Ildefonso Marin-Montesinos,[†] Anil P. Jagtap,[‡] Thomas Halbritter,[‡] Johan van Tol,[§] Sabine Hediger,[†] Daniel Lee,[†] Snorri Th. Sigurdsson,[‡] and Gaël De Paëpe*[†]

[†]Univ. Grenoble Alpes, CEA, CNRS, INAC-MEM, F-38000 Grenoble, France

[‡]Department of Chemistry, University of Iceland, Science Institute, Dunhaga 3, 107 Reykjavik, Iceland

[§]EMR National High Magnetic Field Laboratory, 1800 E. Paul Dirac Drive, Tallahassee, Florida 32310, United States

[‖]CIMAR/NMR National High Magnetic Field Laboratory, 1800 E. Paul Dirac Drive, Tallahassee, Florida 32310, United States

Contents

We introduce a new family of efficient polarizing agents for advanced DNP-NMR applications, composed of two asymmetric bis-nitroxides, in which piperidine-based radicals, a pyrrolinoxyl radical and/or a proxyl radical are linked with a short tether. **Table S1** shows the base biradical molecules that were synthetized in this work. The molecules were first tested in DMSO-d_6/D$_2$O/H$_2$O mixture. **AsymPol** gave the best results in these initial tests. This was expected from the simulations since the relative orientation between the two nitroxide moieties in the case of AsymPol corresponds to a ~90° shift in the β Euler angle. Note that such orientation was originally proposed by the Griffin group since it corresponds to the *b*T*b*K case.[1] In the case of AsymPol, this favourable relative orientation is the result of combined effects: first, the six-membered ring cannot rotate freely around the N-C bound and the lowest energy is obtained when the proton in alpha of the amide is roughly opposite to the amide proton; second, the presence of a carbon-carbon double bound conjugated with the carbonyl of the amide (as opposed to AsymPol II-IV) maintains a favorable relative orientation between the two nitroxide moieties.[1–3] Hence, we chose to concentrate our effort on this molecule, and on a water-soluble version, dubbed **AsymPolPOK**. The other molecules will be further investigated in the near future.

Table S1. Synthesized AsymPol-family molecules and the DNP parameters obtained for 10 mM biradical in DMSO-d_6/H$_2$O (80/20: v/v) or DMSO-d_6/D$_2$O/H$_2$O (80/10/10: v/v) for AsymPol, recorded at 9.4 T, 110 K, and with a MAS rate of 10 kHz. AsymPol IV and AsymPol V were not tested.

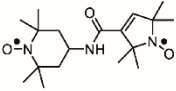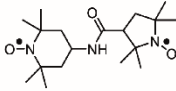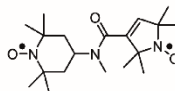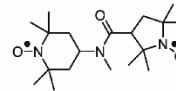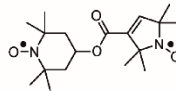|	AsymPol	AsymPol II	AsymPol III	AsymPol IV	AsymPol V
$^1H\varepsilon_{on/off}$	45	14	7.5	–	not soluble
^1HT_B / s	0.7	0.7	2.2	–	

Figure S1 represents the X-band EPR spectra in in 1,2-dichloroethane and their corresponding fits for each biradicals. All the radicals of the family present the characteristic features of nitroxide biradicals with an exchange interaction of the same order of magnitude as the ^{14}N hyperfine coupling. The fitting parameters are reported in **Table S2**. The exchange interaction is significant for each biradical and ranges from 70 to 110 MHz.

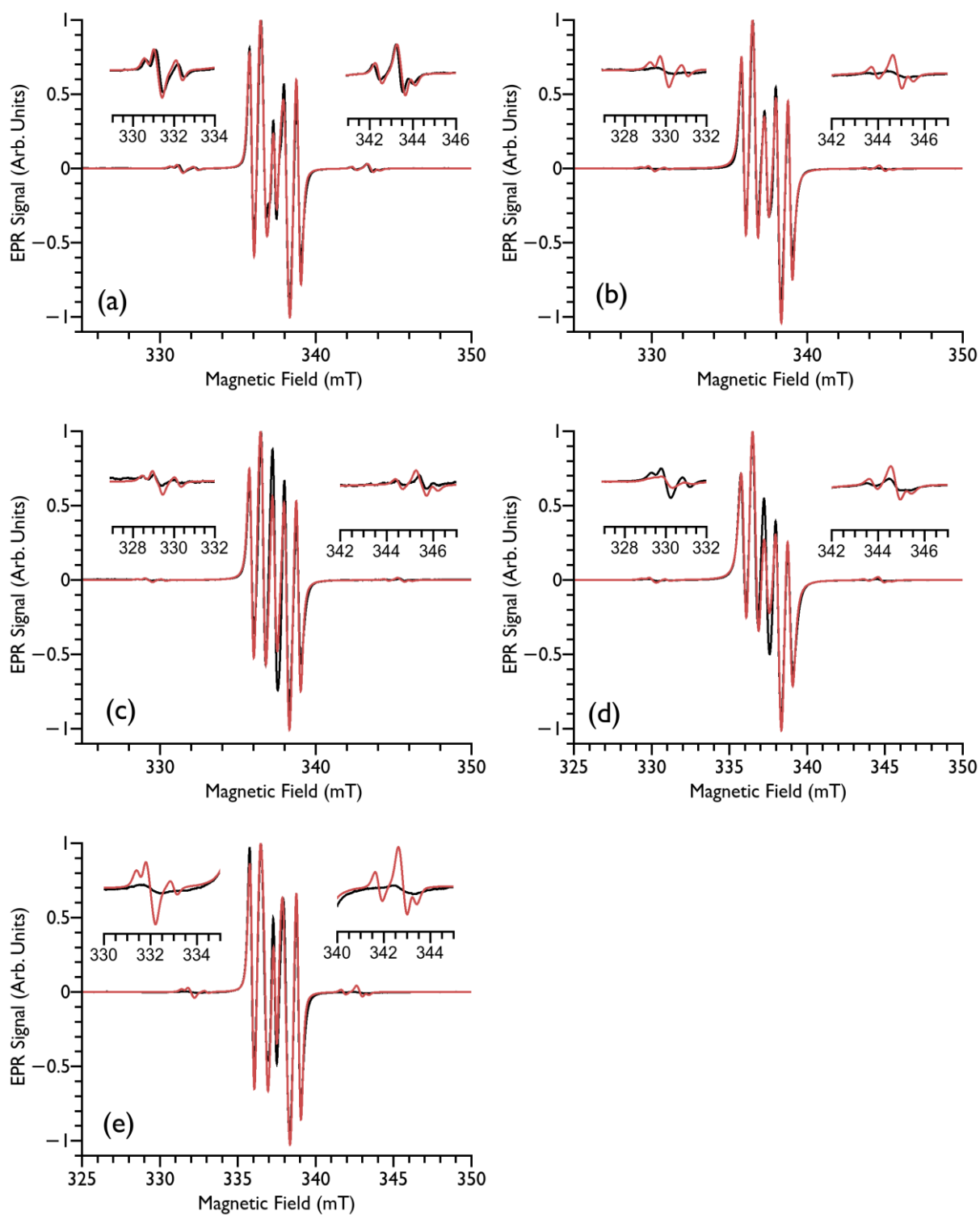**Figure S1**. EPR spectra of the AsymPol family in 1 mM solution in 1,2-dichloroethane (degassed using Argon bubbling for 3 minutes) and their corresponding fit. (a) AsymPol - |J|=80.5 MHz, (b) AsymPol II - |J|= 100 MHz, (c) AsymPol III – J = 111.5 MHz, (d) AsymPol IV - |J| = 99 MHz, (e) AsymPol V - |J|=70 MHz

Table S2: EPR parameters obtained from the fitting of the experimental data

Parameter	AsymPol	AsymPol II	AsymPol III	AsymPol IV	AsymPol V
Isotropic g	[2.0060;2.0062]	[2.0060;2.0062]	[2.0060;2.0062]	[2.0059;2.0062]	[2.0060;2.0062]
Isotropic ^{14}N Hyperfine (MHz)	[39.5, 44]	[39;44.6]	[39;0,45]	[39, 44]	[39 44.3]
Exchange interaction (MHz)	80.5	100	111.5	99	70
Voigtian broadening	[0.23,0.12]	[0.16,0.21]	[0.19,0.17]	[0.22 0.24]	[0.23, 0.12]

Biradical's concentration effect

The performance of **AsymPol** and **AsymPolPOK** have been tested at two different biradical concentrations, 5 and 10 mM. The results are presented in **Figure S2**. For both concentrations, **AsymPol**, **AsymPolPOK** and **AMUPol** provide almost identical performance in terms of relative sensitivity gain $\epsilon_B \times (T_B)^{-1/2}$.
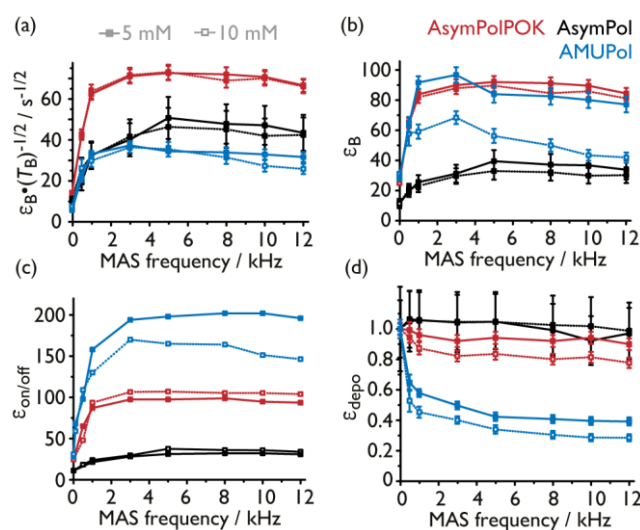

Figure S2. Experimental performance of **AsymPol** (black) and **AsymPolPOK** (red), with a comparison to **AMUPol** (blue), as a function of MAS frequency. The data were recorded using 5 (full symbols) and 10 mM (open symbols) biradical in d_6-DMSO/D$_2$O/H$_2$O (8:1:1; v:v) (for **AsymPol**) or d_8-glycerol/D$_2$O/H$_2$O (6:3:1; v:v) (for **AsymPolPOK** and **AMUPol**) at 9.4 T and 105 K. All samples contain 20 mM ^{13}C-urea. Note that **AsymPolPOK** and **AMUPol** data can thus be compared directly since the same DNP matrix was used. The plots show (a) the relative DNP sensitivity (expressed as $\epsilon_B \times (T_B)^{-1/2}$), (b) the proton polarization gain compared to Boltzmann equilibrium, ϵ_B, (c) the ratio between the NMR signal obtained with and without microwave irradiation, $\epsilon_{on/off}$, and (d) the nuclear depolarization, ϵ_{depo}, expressed here as the ratio between the obtained ^{1}H NMR signal integral and that recorded without sample spinning, both in the absence of microwave irradiation. The latter (static case) represents the Boltzmann equilibrium polarization. Lines are added as a guide. The larger errors for AsymPol reflect the very short T_B (see Table 1 of main manuscript).

EPR simulations

Figure S3 shows the solution-state EPR spectrum for **AsymPol**POK and the corresponding fitting of the data. In the present case, **AsymPolPOK** presents a significant exchange interaction that is $|J_{a,b}| \sim 80.5$ MHz.
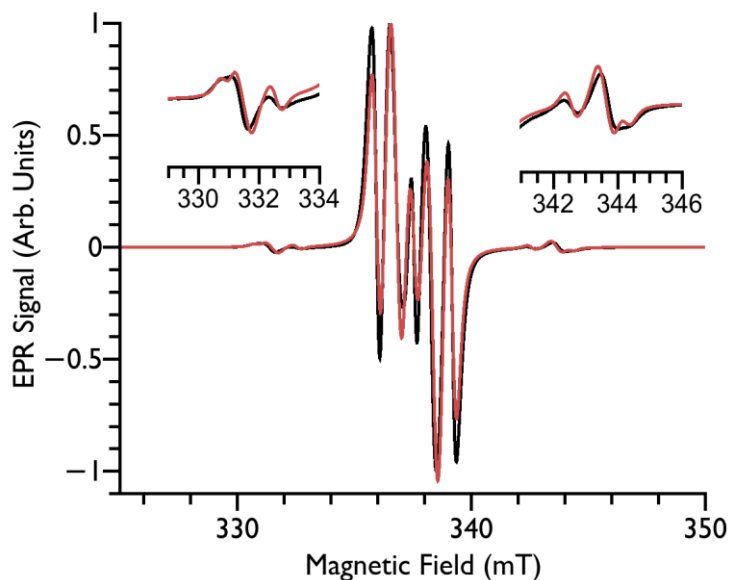

Figure S3. EPR data and associated fit of 1 mM **AsymPolPOK** in water degased with Argon bubbling for 3 minutes. The fitting provides an isotropic $J_{a,b}$ exchange interaction of the order of $|J_{a,b}| \sim 80.5$ MHz. Fitting parameters: g_a=2.0060, g_b=2.0063, A_{za} = 43 MHz, A_{zb} = 47, $|J_{ab}|$ = 80.5 MHz, Voigtian broadening = [[0.15, 0.28] mT. Microwave frequency 9.478 GHz. Note that the magnetic has not been calibrated and therefore the g values are only relative.

AsymPol was crystalized and these data were further used for the EPR calculations.

Collection details: X-ray quality single crystals were obtained by layering n-hexane over an acetone solution of **AsymPol** and crystal were formed within three days. The crystals were isolated from the mother liquor, immediately immersed in cryogenic oil and then mounted. The crystal data was collected using MoKα radiation (λ =0.71073Å) on a Bruker D8Venture (Photon100 CMOS detector) diffractometer equipped with a Cryostream (Oxford Cryosystems) open-flow nitrogen cryostat at the temperature 150.0(2)K. The unit cell determination, data collection, data reduction, structure solution/refinement and empirical absorption correction (SADABS) were carried out using Apex-III (Bruker AXS: Madison, WI, 2015). The structure was solved by direct method and refined by full-matrix least squares on F^2 for all data using SHELXTL[4] and Olex2[5] software. The solvent molecules (acetone) were severely disordered and could not fit to any model. PLATON/SQUEEZE[6] was used to refine only the molecule by excluding the disordered solvent electron density, which corresponds to one acetone per molecule. All non-hydrogen atoms were refined anisotropically and the hydrogen atoms were placed in the calculated positions and refined in riding model.

Figure S4 shows the crystal structure of **AsymPol**, which provides the relative orientation of the g-tensors and the dipolar vector.
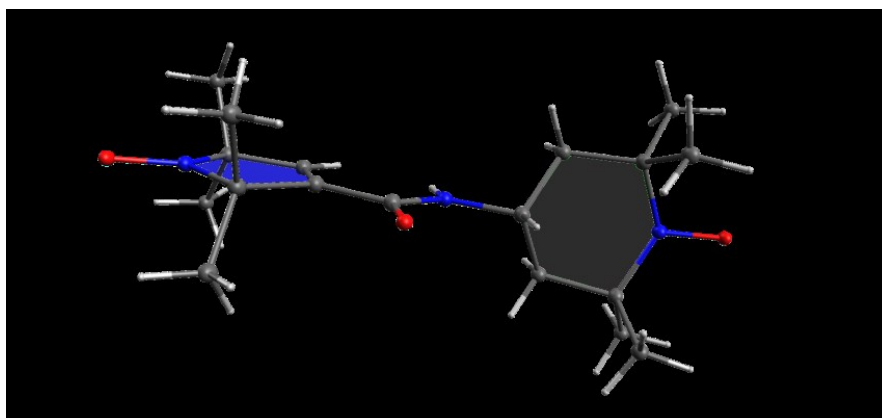

Figure S4. Crystal structure of **AsymPol** obtained by X-ray crystallography.

To obtain the exchange interaction, g-values, and structure of **AsymPolPOK**, we fitted the High Field/Frequency solid-state EPR spectra of 10 mM **AsymPolPOK** in glycerol-d_8/D_2O/H_2O + 20 mM ^{13}C Urea using Easyspin[7], as shown in **Figure S5**. The crystal structure of **AsymPol** was used as input parameters and only the g-values and the exchange interaction were adjusted. The best fit (red) is in agreement with the experimental data (black) as most of the features and relative intensities of the EPR spectrum are reproduced. Nonetheless, the breadth of the experimental spectrum is not fully reproduced, which may indicate that other conformations with larger dipolar/exchange interactions may be present in the frozen sample. The corresponding g-values, g-relative orientation, dipolar interaction, dipolar vector, and exchange interaction are reported in Table S2.
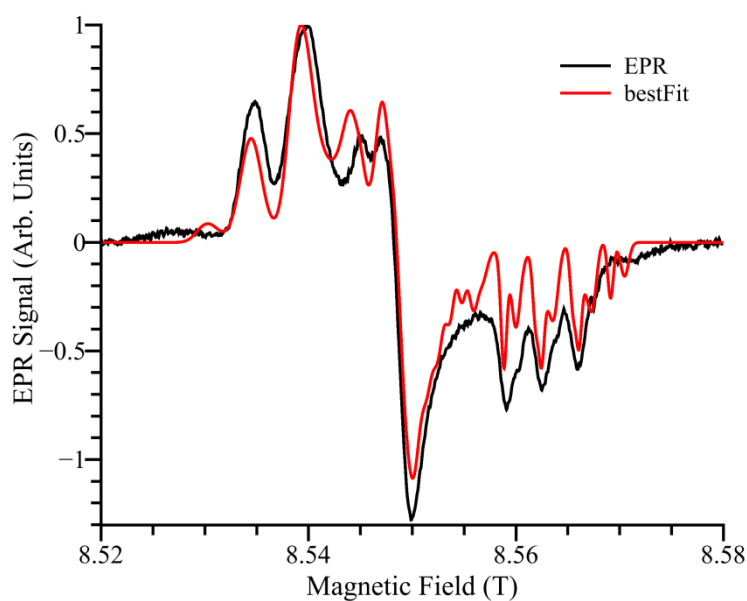

Figure S5. Experimental spectrum (black) of 10 mM AsymPolPOK in glycerol-d_8/D_2O/H_2O (60/30/10 v/v) + 20 mM ^{13}C-urea. The spectrum was recorded at 110 K, with a field modulation of 0.3 mT. The best fit obtained via Easyspin using the X-ray structure as input is also shown (red).

Table S3: AsymPol biradical geometry obtained from the X-Ray structure [a] and after fitting the EPR line [b].

g values [gxx, gyy, gzz] [b]	Euler angles g tensor [a]	Dipolar interaction [a]/ Exchange interaction (-$2J_{a,b}S_aS_b$) [b] (MHz)	Dipolar vector (θ, ϕ)	[14]N Hyperfine coupling (MHz)[8,9]	g- strain
[2.0084 2.0062 2.0024]; [2.0090 2.0060 2.0021];	[106.2619 86.1634 -86.1275]	56/-70	[89.2489 -139.3497]	[13 13 98; 18, 18, 100]	[0.50, 0.49 0.12]*10^{-3}

MAS-DNP simulations

The simulations were performed using codes developed previously[2,10–12]. Except specified otherwise, the parameters used in the computations are $\omega_1 = 2\pi \times 0.4$ MHz, $T_{1,e}^{(b)} = 0.1$ ms[13], $T_{1,e}^{(b)} = 0.4$ ms[13], $T_{2,e}^{(a/b)} = 2$ µs, $T_{1,n} = 4$ s, $A_{a,n} = 2\pi \times [-1 - 1\ 2]$ MHz. $T = 100$ K, $\omega_r = 2\pi \times 8$ kHz where notations are defined in references [12,14]. In **Figure 3**, the microwave frequency / magnetic field was fixed to either $\omega_{\mu w} = 2\pi \times 263.45$ GHz / B$_0$ = 9.394 T, or $\omega_{\mu w} = 2\pi \times 526.9$ GHz / B$_0$ = 18.788 T.

The quality of the parameters extracted from the EPR fit was assessed by comparing the simulated DNP field profile to the experimental data recorded for **AsymPolPOK** (at ~14.1 T and ~110 K with 8 kHz spinning frequency). As shown in **Figure S6**, the agreement between simulation and experiment is good. Thus, we assume in the following that **AsymPolPOK** has an electron-electron dipolar coupling of ~56 MHz and a $J_{a,b}$ exchange interaction of ~-70 MHz, which is close to the $|J_{a,b}| \sim 80.5$ MHz extracted from the liquid-state EPR. Such strong dipolar and exchange interactions explain the relatively fast hyperpolarization build-up times observed with **AsymPolPOK**, as predicted in reference [14].
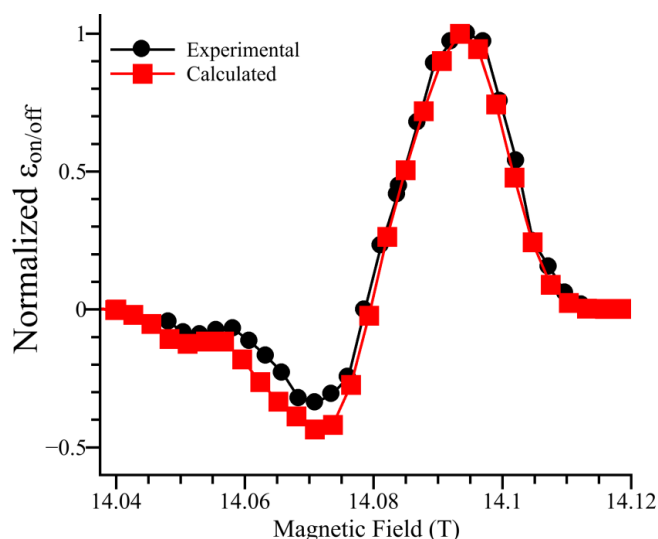

Figure S6. In black, experimental MAS-DNP field profile of 10mM **AsymPolPOK** in glycerol-d$_8$/D$_2$O/H$_2$O (60/30/10 v/v/v) + 20 mM ^{13}C-urea for a MAS rate of 8 kHz, and a temperature of 110 K. In red, calculated MAS-DNP field profile using the following parameters, $\omega_{\mu w} = 2\pi \times 395.175$ GHz.

To complement the theoretical results presented in the manuscript, we performed a series of simulations using the biradical geometry derived from the EPR fit. **Figures S7** and **S8** show the MAS dependence of the polarization gain ϵ_B and of the depolarization ϵ_{Depo} for various $J_{a,b}$ exchange interactions ranging from 0 to 150 MHz, computed either at $B_0 = 9.394$ T (400 MHz ^{1}H NMR) in **Figure S7**, or at $B_0 = 18.788$ T (800 MHz ^{1}H NMR) in **Figure S8**.
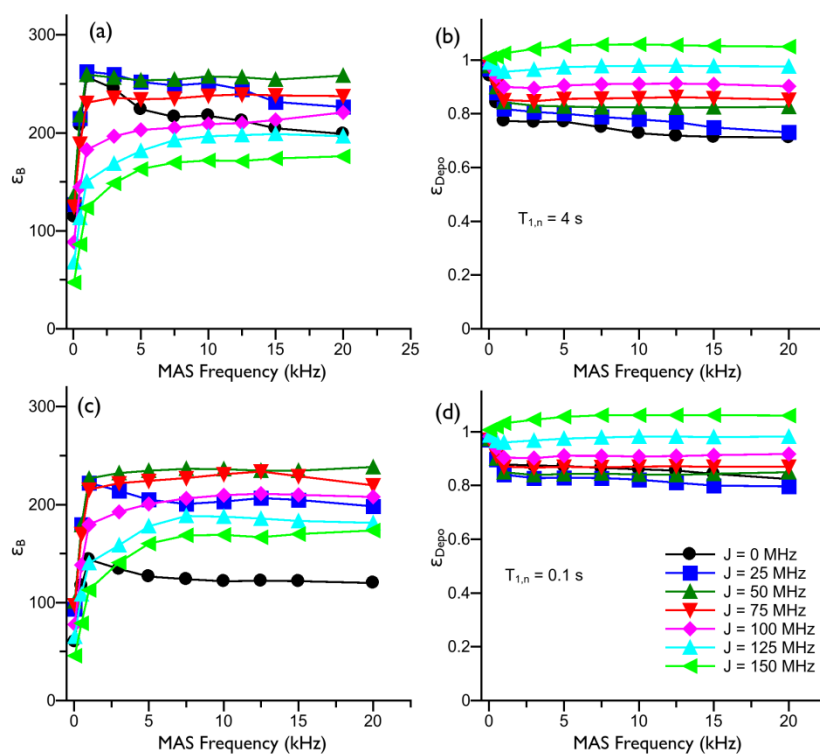

Figure S7. Calculated MAS dependence of ϵ_B (a)/(c) and ϵ_{Depo} (b)/(d) for different exchange interaction strengths: black circles $J_{a,b} = 0$, blue squares $J_{a,b} = -2\pi \times 25$ MHz , green triangles $J_{a,b} = -2\pi \times 50$ MHz, red down pointing triangles $J_{a,b} = -2\pi \times 75$ MHz, pink diamonds $J_{a,b} = -2\pi \times 100$ MHz, light blue triangles $J_{a,b} = -2\pi \times 125$ MHz, green left pointing triangles $J_{a,b} = -2\pi \times 150$ MHz. Figure (a-b) corresponds to a nuclear relaxation time of 4 s, (c-d) corresponds to $T_{1,n} = 0.1$ s. The experimental parameter are $\omega_{\mu w} = 2\pi \times 263.45$ GHz/B$_0$ = 9394 T, T= 100 K.

More precisely, **Figure S7** shows the polarization gain ϵ_B and the depolarization factor ϵ_{Depo} for two sets of nuclear relaxation times, $T_{1n} = 0.1$ and 4 s, respectively. In each case, the electron-electron polarization difference available to hyperpolarize (in presence of μw) or depolarize (in absence of μw) the proton is the same. For relatively long T_{1n} values, the proton polarization can fully equilibrate with the electron-electron polarization difference, whereas for shorter T_{1n} values, this is not the case. In each instance, the depolarization effect is reduced by increasing the J exchange interaction. Another striking point is that the polarization gain is more robust with respect to increased spinning frequencies for larger J exchange interaction values. This observation is consistent with the experimental results as well as previously published results[2,12,14]: as the dipolar/exchange interaction is increased, the electron-electron rotor-events become more efficient and allow maintaining the electron polarization difference, leading to a reduced MAS dependence (in presence of microwave irradiation) and reduced depolarization (in absence of microwave irradiation). Larger exchange interactions also increase the efficiency of the CE rotor-events and thus reduce the DNP build-up time. If this DNP build-up time becomes smaller than the ^{1}H T_{1n}, then the ^{1}H polarization can fully equilibrate with the electron-electron polarization difference. If not, then the ^{1}H polarization only reaches

an intermediate value. Finally, it is important to stress that the presence of too large exchange interactions (i.e. >100 MHz at 9.4 T) reduces the observed polarization gain since it strongly impacts the CE matching conditions, as explained previously.[12,15,16]
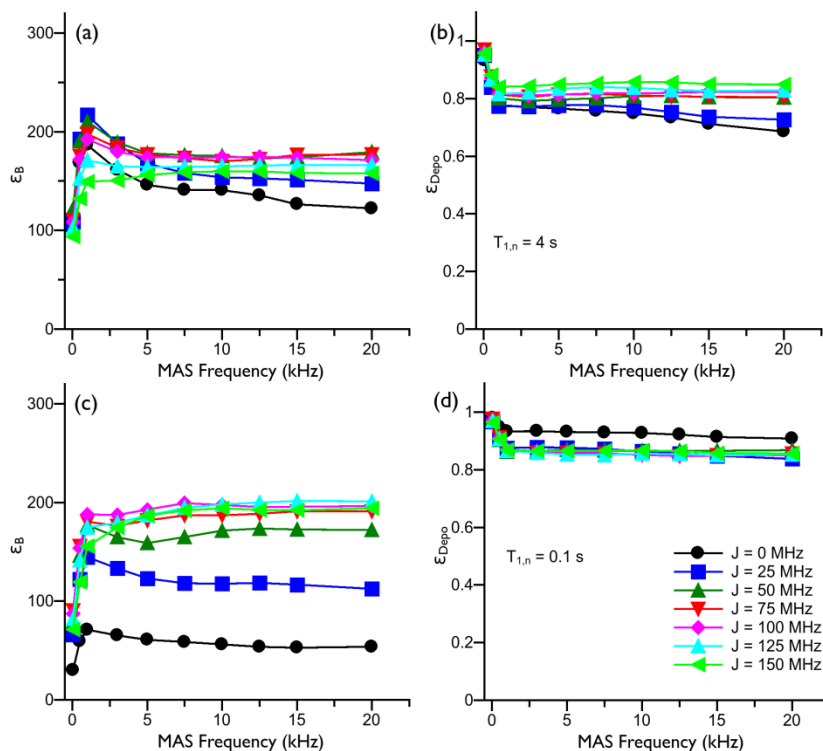

Figure S8. Calculated MAS dependence of ϵ_B (a)/(c) and ϵ_{Depo} (b)/(d) for different exchange interaction strengths: black circles $J_{a,b} = 0$, blue squares $J_{a,b} = -2\pi \times 25$ MHz , green triangles $J_{a,b} = -2\pi \times 50$ MHz, red down pointing triangles $J_{a,b} = -2\pi \times 75$ MHz, pink diamonds $J_{a,b} = -2\pi \times 100$ MHz, light blue triangles $J_{a,b} = -2\pi \times 125$ MHz, green left pointing triangles $J_{a,b} = -2\pi \times 150$ MHz. Figure (a-b) corresponds to a nuclear relaxation time of 4 s, (c-d) corresponds to $T_{1,n}$ = 0.1 s. The experimental parameter are $\omega_{\mu w} = 2\pi \times 526.9$ GHz/B_0 = 18788 T, T = 100 K.

Similar observations can be made at higher magnetic field (18.8 T), as shown in **Figure S8**. The presence of a large J exchange interaction increases the polarization gain while minimizing the depolarization effect, especially for short ^{1}H T_{1n}. The highest exchange interaction computed here (150 MHz) is still efficient at 18.8 T since it does not modify significantly the EPR lineshape, and thus CE matching conditions, at this high magnetic field. This is similar to the results obtained on TEMTriPol-1.[12]

To illustrate this impact of very large J exchange interaction on the shape of the DNP field profile, we report in **Figure S9** the DNP field profile at 9.4 and 18.8 T using (a) $\omega_{\mu w}/2\pi = 263.45$ GHz, (b) $\omega_{\mu w}/2\pi = 529.6$ GHz respectively. As expected, the shape of the DNP field profile is impacted by the size of the exchange interaction, most notably in the negative enhancement region. The DNP efficiency collapses when $2J$ reaches the ^{1}H Larmor frequency $(\omega_{0,1H})/2\pi$, i.e. when $|J_{a,b}| \sim 200$ MHz at 9.4 T. Such behaviour is in agreement with previous work[12,15] and with historical predictions.[16]
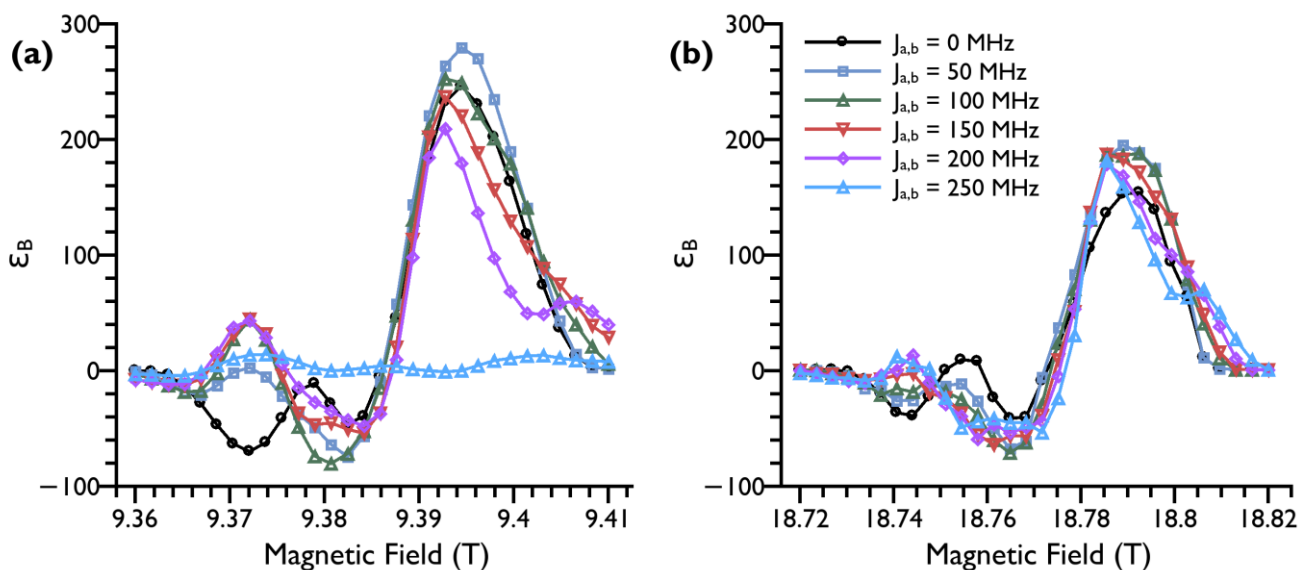
Figure S9. Calculated DNP field profile for different exchange interaction strengths: black circles $J_{a,b} = 0$, blue squares $J_{a,b} = -2\pi \times 50$ MHz, green triangles $J_{a,b} = -2\pi \times 100$ MHz, red down pointing triangles $J_{a,b} = -2\pi \times 150$ MHz, pink diamonds $J_{a,b} = -2\pi \times 200$ MHz, light blue triangles $J_{a,b} = -2\pi \times 250$ MHz. (a) $\omega_{\mu w}/2\pi = 263.45$ GHz, (b) $\omega_{\mu w}/2\pi = 529.6$ GHz

X-ray Crystal structure (xyz coordinates)

55

O	16.71761	13.70126	4.80950
C	16.41368	16.09939	4.80950
N	17.23069	14.86478	4.80950
C	15.56813	16.13988	6.07055
C	15.56813	16.13988	3.54845
H	15.03113	16.95920	6.07729
H	15.03113	16.95920	3.54172
H	16.15392	16.12631	6.85739
H	16.15392	16.12631	2.76161
H	14.97591	15.36014	6.09171
H	14.97591	15.36014	3.52729
O	16.03934	18.97470	4.80950
N	18.22233	19.42818	4.80950
H	19.03452	19.09204	4.80950
C	18.68295	15.07921	4.80950
C	18.71931	16.57496	4.80950
C	17.51737	17.13153	4.80950
C	18.73817	21.46255	3.58596

C	18.73817	21.46255	6.03304
H	18.33047	21.05692	2.77893
H	18.33047	21.05692	6.84007
H	19.69715	21.21337	3.59558
H	19.69715	21.21337	6.02342
C	18.07255	20.88022	4.80950
H	17.10184	21.11904	4.80950
C	17.19457	18.59207	4.80950
C	19.30578	14.47019	6.07632
C	19.30578	14.47019	3.54268
H	19.18177	13.49879	6.06574
H	19.18177	13.49879	3.55326
H	18.86886	14.84706	6.86893
H	18.86886	14.84706	2.75007
H	20.26314	14.67680	6.10133
H	20.26314	14.67680	3.51767
C	18.62682	22.98545	3.48208
C	18.62681	22.98545	6.13692
O	19.02278	24.88545	4.80950
N	18.88681	23.59907	4.80950
C	17.24703	23.40719	3.00979
C	17.24703	23.40719	6.60922
H	17.18927	24.38618	3.00113
H	17.18927	24.38618	6.61787
H	16.56806	23.04481	3.61867
H	16.56806	23.04481	6.00033
H	17.09034	23.06322	2.10560
H	17.09034	23.06322	7.51340
C	19.70175	23.48265	2.50383
C	19.70175	23.48265	7.11517
H	19.51999	23.12764	1.60926
H	19.51999	23.12764	8.00974
H	20.58296	23.17596	2.80394
H	20.58295	23.17596	6.81506
H	19.69024	24.46210	2.47497
H	19.69024	24.46210	7.14403
H	19.59564	17.12001	4.80950

Syntheses of AsymPol family of biradicals

Abbreviations

CDI	Carbonyldiimidazole
DCC	*N*,*N*'-Dicyclohexylcarbodiimide
DMAP	4-Dimethylaminopyridine
EPR	Electron paramagnetic resonance
Et$_3$N	Triethylamine
HOBt	Hydroxybenzotriazole
HRMS	High-resolution mass spectrometry
PMA	Phosphomolybdic acid
TBAF	Tetra-*n*-butylammonium fluoride
*t*BuOOH	Tert-butyl hydroperoxide
TBDMS-Cl	Tert-butyldimethylsilyl chloride
TFA	Trifluoroacetic acid
THF	Tetrahydrofuran
TLC	Thin layer chromatography

Synthetic procedures

General materials and methods

Chemicals were purchased from Sigma-Aldrich Chemical Company and Acros and were used without further purification. Dichloromethane, acetonitrile, and pyridine were freshly distilled over calcium hydride before use; Et$_3$N was purchased anhydrous and stored over potassium hydroxide pellets. Thin layer chromatography (TLC) was performed on glass backed TLC plates with extra hard layer (Kieselgel 60 F$_{254}$, 250 μm, Silicycle) and compounds were visualized by UV light. Silica gel (230-400 mesh, 60 Å) was purchased from Silicycle, and used for flash chromatography. Nitroxide radicals show significant broadening in NMR spectra and loss of NMR signals due to their paramagnetic nature[17,18] and therefore we only report their EPR spectra. All moisture-sensitive reactions were carried out in oven-dried glassware using nitrogen or argon from standard BOC industrial cylinders, dried through an activated silica column. Molecular mass of the new organic compounds was determined by HRMS (Bruker, MicroTof-Q). Purity of **AsymPol (3)**, **AsymPol II (5)**, **AsymPol III (7)**, **AsymPol IV (8)**, **AsymPol V (10)**, **13** and **AsymPolPOK (17)** were analysed on GL Sciences Inertsustain C18 4.6 × 150 mm analytical column with UV detection at λ = 254 nm on Beckman Coulter Gold HPLC system. Analytical HPLC run (Flow rate = 1 mL/min): Solvent A, 0.1% TFA in water; solvent B, 0.1% TFA in MeCN; 0-2 min isochratic 10% B, 2-12 min gradient 10%-100% B, 12-14 min isochratic 100% B, 14-16 min 100%-10% B

Synthetic protocols
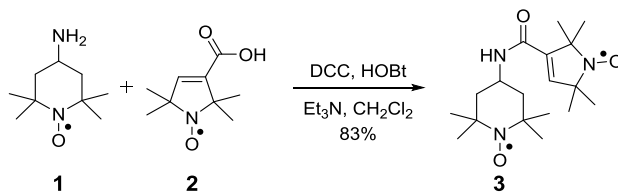
AsymPol (3)

To a solution of **2**[19] (0.032 g, 0.18 mmol) in CH_2Cl_2 (4 mL) was added DCC (0.039 g, 0.19 mmol), HOBt (0.053 g, 0.35 mmol) and Et_3N (0.073 mL, 0.53 mmol) under an inert atmosphere of argon. After stirring for 15 min, **1**[20] (0.030 g, 0.18 mmol) was added. The resulting solution was stirred at 25 °C for 12 h, diluted with CH_2Cl_2 (10 mL) and washed successively with sat. aqueous solution of $NaHCO_3$ (1x10 mL) and brine (1x10 mL). The organic layer was concentrated *in vacuo* and the crude product was purified by flash column chromatography (silica) using a gradient elution (EtOAc:pet ether; 0:100 to 30:70) to give **3** (0.049 g, 83% yield) as an orange solid.

TLC (Silica gel, 10% MeOH in CH_2Cl_2), R_f (**1**) = 0.2, R_f (**2**) = 0.8, R_f (**3**) = 0.9, PMA active.

    (Silica gel, 2.5% MeOH in CH_2Cl_2), R_f (**3**) = 0.3

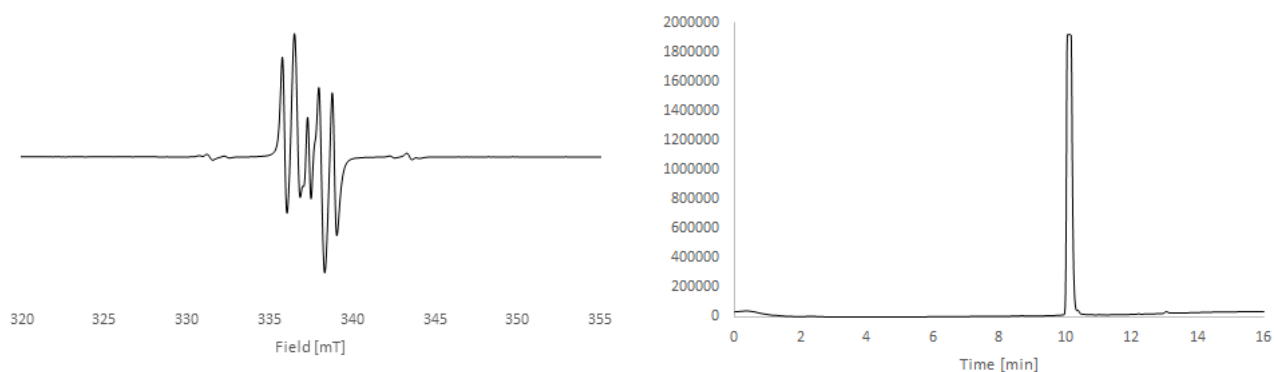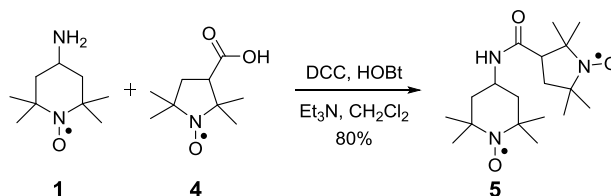HRMS: calculated for $C_{18}H_{31}N_3O_3$: 337.2365, found 339.2520 $(M+2H)^{2+}$.

Figure S10. EPR spectrum of compound **3** (**AsymPol**) in 1,2 dichloroethane at 25 °C. (left) and HPLC chromatogram (right).

AsymPol II (5)

To a solution of **4**[21] (0.032 g, 0.18 mmol) in CH_2Cl_2 (4 mL) was added DCC (0.039 g, 0.19 mmol), HOBt (0.053 g, 0.35 mmol) and Et_3N (0.073 mL, 0.53 mmol) under an inert atmosphere of argon. After stirring for 15 min, **1**[20] (0.030 g, 0.18 mmol) was added. The resulting solution was stirred at 25 °C for 12 h, diluted with CH_2Cl_2 (10 mL) and washed successively with sat. aqueous solution of $NaHCO_3$ (1x10 mL) and brine (1x10 mL). The organic layer was concentrated *in vacuo* and the crude product was purified by flash column chromatography (silica) using a gradient elution (EtOAc:pet ether; 0:100 to 35:65) to give **5** (0.047 g, 80% yield) as a yellow solid.

TLC (Silica gel, 40% EtOAc in pet ether), R_f (**4**) = 0.4, R_f (**5**) = 0.2, PMA active.

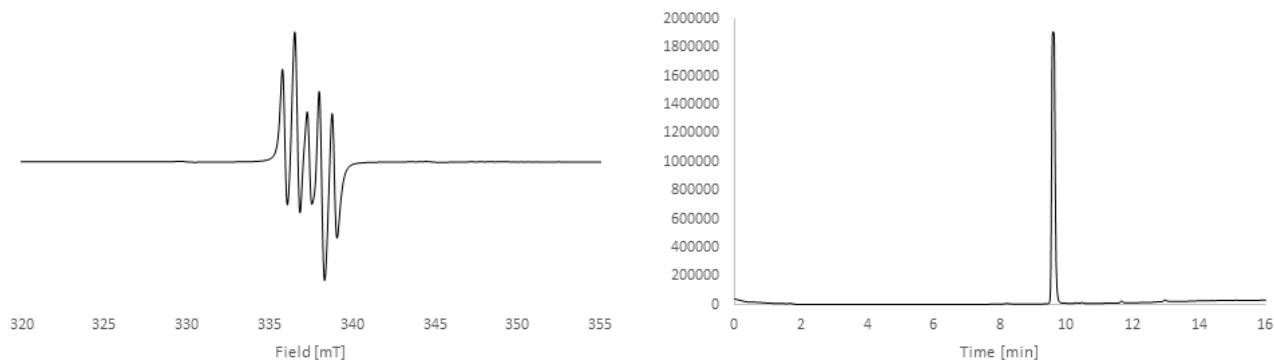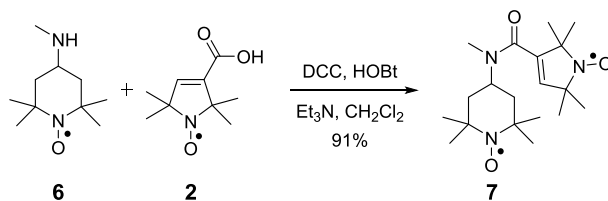HRMS: calculated for $C_{18}H_{33}N_3O_3$: 339.2522, found 340.2665 (M+H)$^+$.

Figure S11. EPR spectrum of compound **5** (**AsymPol II**) in 1,2 dichloroethane at 25 °C (left) and HPLC chromatogram (right).

AsymPol III (7)

To a solution of **2**[19] (0.030 g, 0.16 mmol) in CH_2Cl_2 (4 mL) was added DCC (0.037 g, 0.18 mmol), HOBt (0.049 g, 0.32 mmol) and Et_3N (0.070 mL, 0.50 mmol) under an inert atmosphere of argon. After stirring for 15 min, **6**[20] (0.030 g, 0.16 mmol) was added. The resulting solution was stirred at 25 °C for 12 h, diluted with CH_2Cl_2 (10 mL) and washed successively with sat. aqueous solution of $NaHCO_3$ (1x10 mL) and brine (1x10 mL). The organic layer was concentrated *in vacuo* and the crude product was purified by flash column chromatography (silica) using a gradient elution (EtOAc:pet ether; 0:100 to 35:65) to give **7** (0.051 g, 91% yield) as a yellow solid.

TLC (Silica gel, 40% EtOAc in pet ether), R_f (**2**) = 0.3, R_f (**7**) = 0.2, PMA active.

HRMS: calculated for $C_{19}H_{33}N_3O_3$: 351.2522, found 353.2673 (M+2H)$^{2+}$.
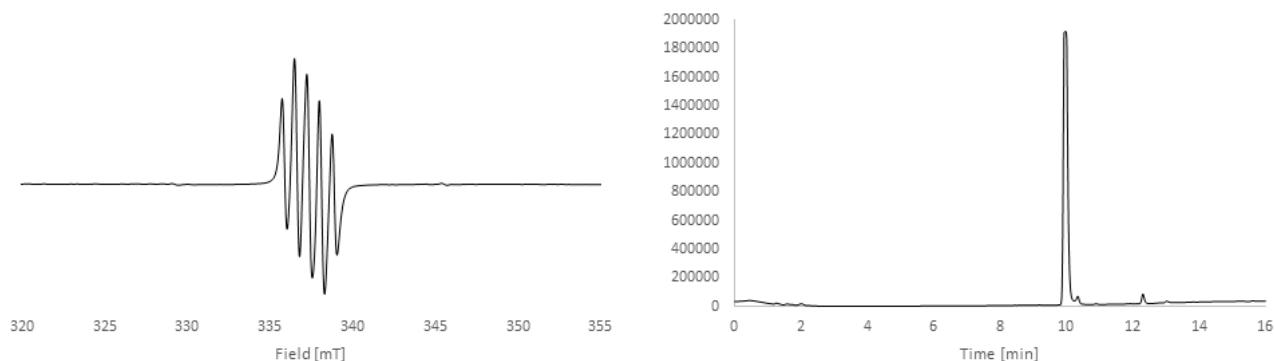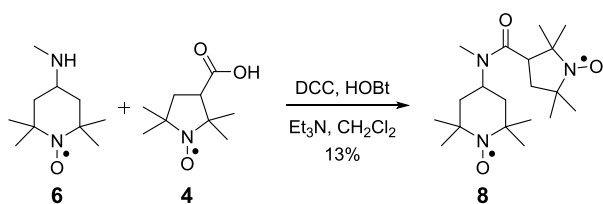

Figure S12. EPR spectrum of compound **7** (**AsymPol III**) in 1,2 dichloroethane at 25 °C (left) and HPLC chromatogram (right).

AsymPol IV (8)

To a solution of 4[21] (0.120 g, 0.65 mmol) in CH_2Cl_2 (7 mL) was added DCC (0.146 g, 0.71 mmol), HOBt (0.198 g, 1.29 mmol) and Et_3N (0.270 mL, 1.94 mmol) under an inert atmosphere of argon. After stirring for 15 min, 6[20] (0.120 g, 0.65 mmol) was added. The resulting solution was stirred at 25 °C for 12 h, diluted with CH_2Cl_2 (10 mL) and washed successively with sat. aqueous solution of $NaHCO_3$ (1x10 mL) and brine (1x10 mL). The organic layer was concentrated *in vacuo* and the crude product was purified by flash column chromatography (silica) using a gradient elution (EtOAc:pet ether; 0:100 to 35:65) to give 8 (0.028 g, 13% yield) as a yellow solid.

TLC (Silica gel, 40% EtOAc in pet ether), R_f (4) = 0.4, R_f (8) = 0.2, PMA active.

HRMS: calculated for $C_{19}H_{35}N_3O_3$: 353.2678, found 354.2778 (M+H)$^+$.
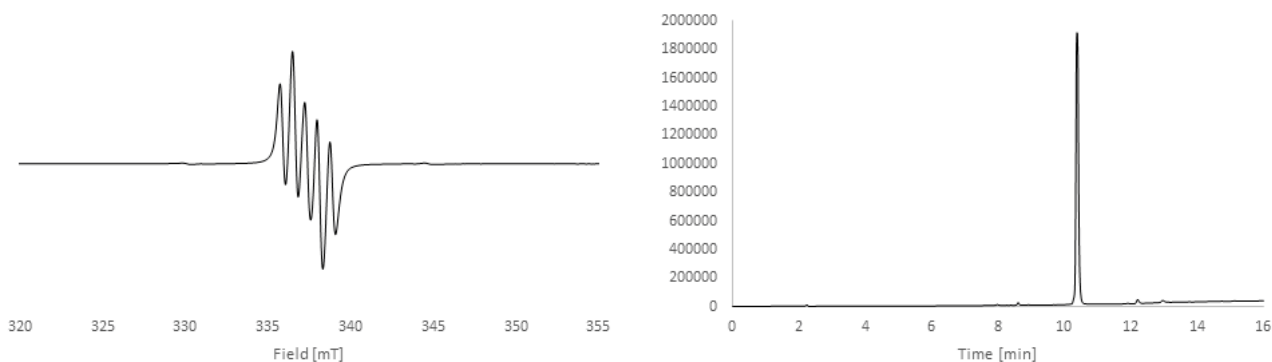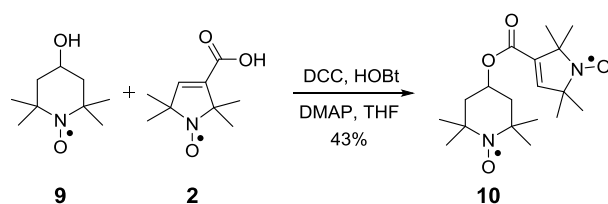

Figure S13 EPR spectrum of compound 8 (**AsymPol IV**) in 1,2 dichloroethane at 25 °C (left) and HPLC chromatogram (right).

AsymPol V (10)

To a solution of **2**[19] (0.060 g, 0.33 mmol) in THF (6 mL) was added DCC (0.087 g, 0.42 mmol), HOBt (0.057 g, 0.42 mmol) and DMAP (0.230 g, 0.20 mmol) under an inert atmosphere of argon. After stirring for 15 min, **9** (0.068 g, 0.39 mmol) was added. The resulting solution was stirred at 25 °C for 12 h. Solvent was removed *in vacuo*. The residue was diluted with CH_2Cl_2 (10 mL) and washed successively with sat. aqueous solution of $NaHCO_3$ (1x10 mL) and brine (1x10 mL). The organic layer was concentrated *in vacuo* and the crude product was purified by flash column chromatography (silica) using a gradient elution (EtOAc:pet ether; 0:100 to 20:80) to give **10** (0.048 g, 43% yield) as a yellow solid.

TLC (Silica gel, 20% EtOAc in pet ether), R_f (**2**) = 0.3, R_f (**10**) = 0.2, PMA active.

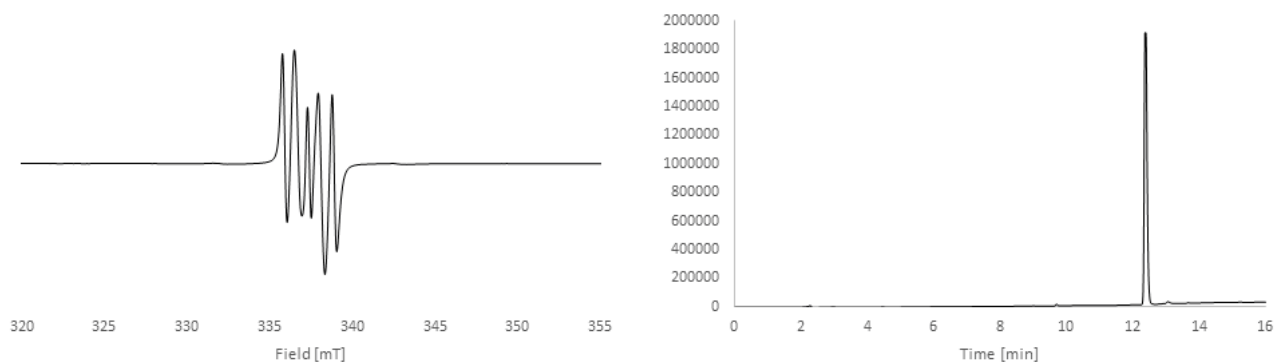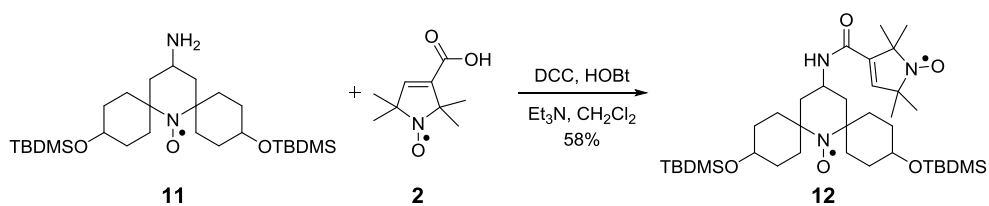HRMS: calculated for $C_{18}H_{30}N_2O_4$: 338.4480, found 361.2096 (M+Na)$^+$.

**Figure S14.** EPR spectrum of compound **10** (**AsymPol V**) in 1,2 dichloroethane at 25 °C (left) and HPLC chromatogram (right).

Compound 12

To a solution of 2^{19} (0.005 g, 0.03 mmol) in CH_2Cl_2 (3 mL) was added DCC (0.006 g, 0.32 mmol), HOBt (0.009 g, 0.06 mmol) and Et_3N (0.013 mL, 0.09 mmol) under an inert atmosphere of argon. After stirring for 15 min, 11^{22} (0.015 g, 0.03 mmol) was added. The resulting solution was stirred at 25 °C for 12 h. The reaction mixture was diluted with CH_2Cl_2 (10 mL) and washed successively with sat. aqueous solution of $NaHCO_3$ (10 mL) and brine (10 mL). The organic layer was concentrated *in vacuo* and the crude product was purified by flash column chromatography (silica) using a gradient elution (EtOAc:pet ether; 0:100 to 30:70) to give **12** (0.011 g, 58% yield) as a yellow solid.

TLC (Silica gel, 3% MeOH in CH_2Cl_2), R_f (**2**) = 0.3, R_f (**12**) = 0.6, PMA active.

HRMS: calculated for $C_{36}H_{67}N_3O_5Si_2$: 677.4619, found 700.4505 (M+Na)$^+$.
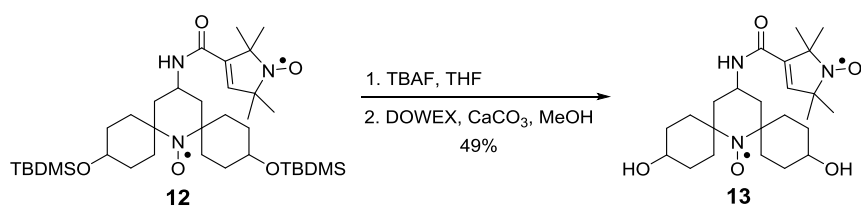
Compound 13

TBAF (0.800 mL, 0.78 mmol, 1 M in THF) was added to a solution of **12** (0.088 g, 0.13 mmol) in anhydrous THF (4 mL). The resulting solution was heated at 60 °C for 12 h, cooled down and the solvent removed *in vacuo*. The residue was dissolved in MeOH (4 mL) and DOWEX (50WX8 hydrogen forms, 200-400 mesh, 0.50 g) and $CaCO_3$ (0.165, 1.65 mmol) were added. The resulting suspension was stirred at 25 °C for 12 h. The reaction mixture was filtered through a bed of celite, the filtrate concentrated *in vacuo* and the crude product was purified by flash column chromatography (silica) using a gradient elution ($MeOH:CH_2Cl_2$; 0:100 to 10:90) to give **13** (0.034 g, 49% yield) as a yellow solid.

TLC (Silica gel, 10% MeOH in CH_2Cl_2), R_f (**11**) = 1, R_f (**13**) = 0.1, PMA active.

HRMS: calculated for $C_{24}H_{39}N_3O_5$: 449.2890, found 472.2774 (M+Na)$^+$.
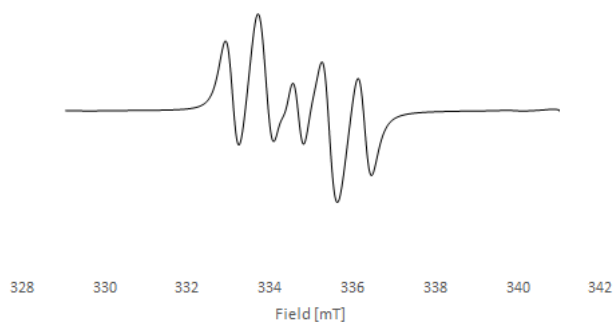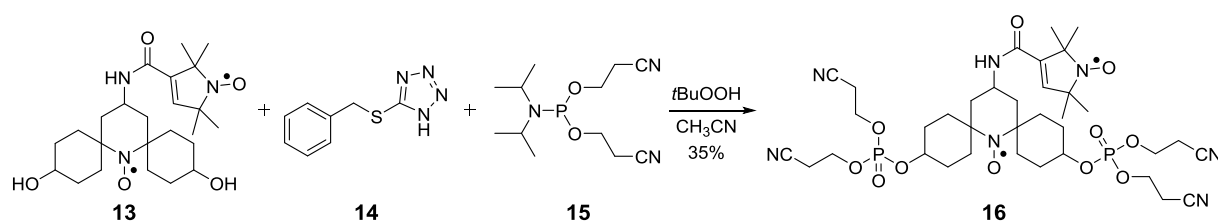

**Figure S15.** EPR spectrum of compound **13** in water at 25 °C.

Compound 16

To a solution of compound **13** (0.045 g, 0.10 mmol) in CH$_3$CN (4 mL) was added **14** (0.058 g, 0.30 mmol) and **15** (0.053 g, 0.35 mmol) under an inert atmosphere of argon. After stirring at 25 °C for 2 h, *t*BuOOH (0.384 mL, 3.20 mmol, 75% in water) was added. The resulting clear solution was stirred at 25 °C for 30 min. The solvent was removed *in* vacuo, the residue obtained was diluted with CH$_2$Cl$_2$ (10 mL) and washed successively with sat. aqueous solution of NaHCO$_3$ (1x10 mL) and brine (1x10 mL). The organic layer was concentrated *in vacuo* and the crude product was purified by flash column chromatography (silica) using a gradient elution (MeOH:CH$_2$Cl$_2$; 0:100 to 3:97) to give **16** (0.028 g, 35% yield) as a yellow solid.

TLC (Silica gel, 10% MeOH in CH$_2$Cl$_2$), R$_f$ (**13**) = 0.4, R$_f$ (**16**) = 0.6, PMA active.

^{31}P-NMR (CDCl$_3$): -3.74, -4.35

HRMS: calculated for C$_{36}$H$_{53}$N$_7$O$_{11}$P$_2$: 821.3278, found 844.3172 (M+Na).
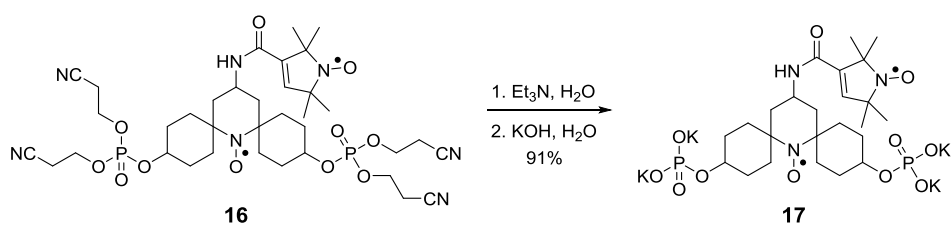
AsymPolPOK (17)

To a solution of **16** (0.045 g, 0.07 mmol) in H_2O (2 mL) was added Et_3N (0.300 mL, 2.14 mmol). The resulting solution was stirred at 60 °C for 12 h. The solvent was removed *in vacuo*. The residue was diluted with H_2O (2 mL) and KOH (0.018 g, 0.33 mmol) was added. The resulting solution was stirred at 60 °C for 12 h. The solvent was removed *in vacuo* to give **17** (0.049 g, 91% yield) as a yellow solid.

TLC (Silica gel, 10% MeOH in CH_2Cl_2), R_f (**16**) = 0.6, R_f (**17**) = 0, PMA active.

^{31}P-NMR (D_2O): -3.23

HRMS: calculated for $C_{24}H_{41}N_3O_{11}P_2$: 609.2216, found 630.1948 (M+Na-2H)$^-$.
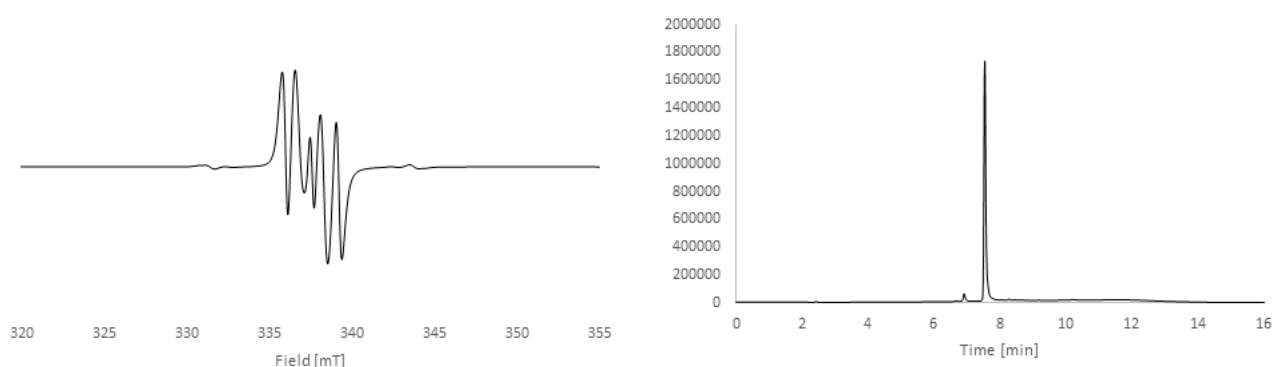

Figure S16. EPR spectrum of **AsymPolPOK** (**17**) in H_2O at 25 °C (left) and HPLC chromatogram (right)

MAS-DNP solid-state NMR experiments

Sample preparation.

The following solutions of **AsymPol**, **AsymPolPOK**, and **AMUPol** were prepared:

1. Two samples of **AsymPol** at concentrations of 5 and 10 mM. The glassy matrix was a mixture of dimethyl sulfoxide-d_6/D_2O/H_2O (8:1:1) containing ^{13}C-urea at a concentration of 20 mM.

2. Two samples of **AsymPolPOK** at concentrations of 5 and 10 mM. The glassy matrix was a mixture of glycerol-d_8/D_2O/H_2O (6:3:1) containing ^{13}C-urea at a concentration of 20 mM.

3. Two samples of **AMUPol** at concentrations of 5 and 10 mM. The glassy matrix was a mixture of glycerol-d_8/D_2O/H_2O (6:3:1) containing ^{13}C-urea at a concentration of 20 mM.

30 µL of each sample was packed in a 3.2 mm sapphire MAS rotor without using a silicone plug, to avoid interference from its NMR signals, and closed with a vespel cap.

The γ-alumina nanopowder was purchased from Sigma-Aldrich and used as received. For a 'DNP ready' sample, the nanopowder was impregnated with 5 mM **AsymPolPOK**, 2 M ^{13}C-urea, d_8-glycerol/D_2O/H_2O (6:3:1; v:v) until the powder became slightly wet. It was then transferred to a 1.3 mm o.d. zirconia rotor and sealed with a vespel drive cap. The 2 M ^{13}C-urea was added to the sample to have a substantial amount of material for internal referencing and pulse calibration.

Experimental procedures and data analysis

The experiments were carried out on Bruker 9.4, 14.1, and 18.8 T DNP-NMR Avance III spectrometers, equipped with low temperature 3.2 mm (and 1.3 mm at 18.8 T) wide-bore MAS probes. For the experiments at 9.4 T, the sample temperature was ~104 K and the following MAS frequencies were used: 0, 0.5, 1, 3, 5, 8, 10, and 12 kHz. {^{1}H-}^{13}C CP-MAS experiments were recorded using 100 kHz nutation for ^{1}H π/2 pulses and heteronuclear decoupling and a ramped (50-100%) power to match a Hartmann-Hahn CP condition when using 50 kHz for ^{13}C nutation during CP spin-locking. Primostrato ^{27}Al NMR spectra were recorded at 18.8 T using {^{1}H-}^{27}Al CP-MAS. For the 1D experiments, a central-transition (CT)-selective (~21 kHz CT nutation) spin-locking of ^{27}Al for 2 ms

was used for CT-CP, whereas for the MQMAS[23–25] experiments a triple-quantum CP step used high power ^{27}Al excitation (~65 kHz nutation) and associated ^{1}H (square) spin-locking to match the Hartmann-Hahn condition for 1 ms. A reconversion pulse (also at 65 kHz) of 1.5 µs was employed before a z-filter of 20 µs and a CT-selective π/2 pulse of 12 µs in the MQMAS experiment. For the sheared spectrum shown in Figure 4, 192 transients were recorded for each of 18 complex (States-TPPI) t_1 increments of 29.47 µs.
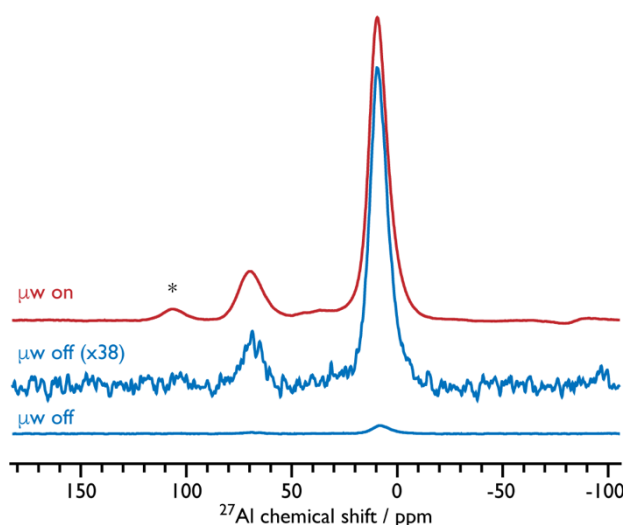

Figure S17. {^{1}H-}^{27}Al CP MAS NMR spectra of γ-alumina, recorded at 18.8 T, a sample temperature of ~125 K, with a MAS frequency of 20 kHz, and with (red) and without (blue) microwave irradiation suitable for DNP. The asterisk denotes a large spinning side band.

To evaluate enhancement factor ($\varepsilon_{on/off}$), the ^{13}C CP-MAS spectra at the different spinning frequencies were registered with (S_{on}^{CP}) and without (S_{off}^{CP}) microwave irradiation, and the enhancement factor is given by:

$$\varepsilon_{on/off} = \frac{S_{on}^{CP}}{S_{off}^{CP}}$$

To evaluate the depolarization factor (ε_{depo}) a careful experimental procedure was performed. Due to the size of the background signal, the procedure proposed by Q. Chen *et al.*[26] has been used to obtain a ^{1}H signal with minimal interference from the ^{1}H background signals from the probe. The procedure requires the acquisition of π/2-pulse and π-pulse ^{1}H spectra in the absence of microwaves, which are used to obtain the sample ^{1}H signal with much

reduced background signals ($S_{\nu kHz}^{nobg}$). The procedure is repeated at each spinning frequency. To further minimize the background signal, the experimental repetition delay (D_1) was short (5 s). Therefore, the obtained data after background suppression (as detailed in reference [16]) was corrected by the T_B, which was measured through saturation-recovery experiments:

$$S_{\nu kHz} = \frac{S_{\nu kHz}^{nobg}}{(1 - e^{-D_1/T_B})}$$

Subsequently, ε_{depo} was calculated by the ratio between the corrected ^1H signal at each MAS frequency ($S\nu_{kHz}$) and the ^1H signal at 0 kHz MAS ($S_{\square kHz}$), as detailed in reference [11].

$$\varepsilon_{depo} = \frac{S_{\nu kHz}}{S_{0kHz}}$$

The enhancements factors were corrected by multiplying $\varepsilon_{on/off}$ by ε_{depo}, obtaining the DNP gain compared to Boltzmann equilibrium ε_B.

$$\varepsilon_b = \varepsilon_{on/off} \times \varepsilon_{depo}$$

The relative sensitivity was evaluated using the following expression:

$$\text{Sensitivity} = \frac{\varepsilon_B}{\sqrt{T_b}}$$

References

(1)   Matsuki, Y.; Maly, T.; Ouari, O.; Karoui, H.; Le Moigne, F.; Rizzato, E.; Lyubenova, S.; Herzfeld, J.; Prisner, T. F.; Tordo, P.; et al. Dynamic Nuclear Polarization with a Rigid Biradical. *Angew. Chemie Int. Ed.* **2009**, *48* (27), 4996–5000.

(2)   Mentink-Vigier, F.; Akbey, U.; Oschkinat, H.; Vega, S.; Feintuch, A. Theoretical Aspects of Magic Angle Spinning - Dynamic Nuclear Polarization. *J. Magn. Reson.* **2015**, *258* (12), 102–120.

(3)   Perras, F. A.; Sadow, A.; Pruski, M. In Silico Design of DNP Polarizing Agents: Can Current Dinitroxides Be Improved? *ChemPhysChem* **2017**, *18* (16), 2279–2287.

(4)   Sheldrick, G. SHELXS/XL. *Acta Crystallogr., Sect. A Fundam. Crystallogr.* **2008**, *46*, 112–122.

(5)   Dolomanov, O. V.; Bourhis, L. J.; Gildea, R. J.; Howard, J. A. K.; Puschmann, H. OLEX2 : A Complete Structure Solution, Refinement and Analysis Program. *J. Appl. Crystallogr.* **2009**, *42* (2), 339–341.

(6)   van der Sluis, P.; Spek, A. L. BYPASS: An Effective Method for the Refinement of Crystal Structures Containing Disordered Solvent Regions. *Acta Crystallogr. Sect. A Found. Crystallogr.* **1990**, *46* (3), 194–201.

(7)   Stoll, S.; Schweiger, A. EasySpin, a Comprehensive Software Package for Spectral Simulation and Analysis in EPR. *J. Magn. Reson.* **2006**, *178* (1), 42–55.

(8)   Bordignon, E. EPR Spectroscopy of Nitroxide Spin Probes. In *eMagRes*; John Wiley & Sons, Ltd: Chichester, UK, 2017; Vol. 6, pp 235–254.

(9)   Hu, K.-N.; Song, C.; Yu, H.; Swager, T. M.; Griffin, R. G. High-Frequency Dynamic Nuclear Polarization Using Biradicals: A Multifrequency EPR Lineshape Analysis. *J. Chem. Phys.* **2008**, *128* (5), 052302.

(10)   Mentink-Vigier, F.; Akbey, U.; Hovav, Y.; Vega, S.; Oschkinat, H.; Feintuch, A. Fast Passage Dynamic Nuclear Polarization on Rotating Solids. *J. Magn. Reson.* **2012**, *224*, 13–21.

(11)   Mentink-Vigier, F.; Paul, S.; Lee, D.; Feintuch, A.; Hediger, S.; Vega, S.; De Paëpe, G. Nuclear Depolarization and Absolute Sensitivity in Magic-Angle Spinning Cross Effect Dynamic Nuclear Polarization. *Phys. Chem. Chem. Phys.* **2015**, *17* (34), 21824–21836.

(12)   Mentink-Vigier, F.; Mathies, G.; Liu, Y.; Barra, A.-L.; Caporini, M. A.; Lee, D.; Hediger, S.; G. Griffin, R.; De Paëpe, G. Efficient Cross-Effect Dynamic Nuclear Polarization without Depolarization in High-Resolution MAS NMR. *Chem. Sci.* **2017**, *8* (12), 8150–8163.

(13)   Sato, H.; Kathirvelu, V.; Fielding, A.; Blinco, J. P.; Micallef, A. S.; Bottle, S. E.; Eaton, S. S.; Eaton, G. R. Impact of Molecular Size on Electron Spin Relaxation Rates of Nitroxyl Radicals in Glassy Solvents between 100 and 300 K. *Mol. Phys.* **2007**, *105* (15–16), 2137–2151.

(14)   Mentink-Vigier, F.; Vega, S.; De Paëpe, G. Fast and Accurate MAS–DNP Simulations of Large Spin Ensembles. *Phys. Chem. Chem. Phys.* **2017**, *19* (5), 3506–3522.

(15)   Mathies, G.; Caporini, M. A.; Michaelis, V. K.; Liu, Y.; Hu, K.-N.; Mance, D.; Zweier, J. L.; Rosay, M.; Baldus, M.; Griffin, R. G. Efficient Dynamic Nuclear Polarization at 800 MHz/527 GHz with Trityl-Nitroxide Biradicals. *Angew. Chem. Int. Ed.* **2015**, *127* (40), 11936–11940.

(16)   Wollan, D. S. Dynamic Nuclear Polarization with an Inhomogeneously Broadened ESR Line. I. Theory. *Phys. Rev. B* **1976**, *13* (9), 3671–3685.

(17)   Li, Y.; Lei, X.; Li, X.; Lawler, R. G.; Murata, Y.; Komatsu, K.; Turro, N. J. Indirect 1H NMR Characterization of H2@C60 Nitroxide Derivatives and Their Nuclear Spin Relaxation. *Chem. Commun.* **2011**, *47* (46), 12527–12529.

(18)   Lee, T. D.; Keana, J. F. W. In Situ Reduction of Nitroxide Spin Labels with Phenylhydrazine in Deuteriochloroform Solution. Convenient Method for Obtaining Structural Information on Nitroxides Using Nuclear Magnetic Resonance Spectroscopy. *J. Org. Chem.* **1975**, *40* (21), 3145–3147.

(19)   Oyaizu, K.; Kawamoto, T.; Suga, T.; Nishide, H. Synthesis and Charge Transport Properties of Redox-Active Nitroxide Polyethers with Large Site Density. *Macromolecules* **2010**, *43* (24), 10382–10389.

(20)   Rosen, G. M. Use of Sodium Cyanoborohydride in the Preparation of Biologically Active Nitroxides. *J. Med. Chem.* **1974**, *17* (3), 358–360.

(21)   Sosnovsky, G.; Cai, Z. A Study of the Favorskii Rearrangement with 3-Bromo-4-Oxo-2,2,6,6-Tetramethylpiperidine-1-Oxyl. *J. Org. Chem.* **1995**, *60* (11), 3414–3418.

(22)   Jagtap, A. P.; Geiger, M.-A.; Stöppler, D.; Orwick-Rydmark, M.; Oschkinat, H.; Sigurdsson, S. T. BcTol: A Highly Water-Soluble Biradical for Efficient Dynamic Nuclear Polarization of Biomolecules. *Chem. Commun.* **2016**, *52* (43), 7020–7023.

(23)   Frydman, L.; Harwood, J. S. Isotropic Spectra of Half-Integer Quadrupolar Spins from Bidimensional Magic-Angle Spinning NMR. *J. Am. Chem. Soc.* **1995**, *117* (19), 5367–5368.

(24)   Medek, A.; Harwood, J. S.; Frydman, L. Multiple-Quantum Magic-Angle Spinning NMR: A New Method for the Study of Quadrupolar Nuclei in Solids. *J. Am. Chem. Soc.* **1995**, *117* (51), 12779–12787.

(25)   Ashbrook, S. E.; Wimperis, S. Multiple-Quantum Cross-Polarization and Two-Dimensional MQMAS NMR of Quadrupolar Nuclei. *J. Magn. Reson.* **2000**, *147* (2), 238–249.

(26)   Chen, Q.; Hou, S. S.; Schmidt-Rohr, K. A Simple Scheme for Probehead Background Suppression in One-Pulse 1H NMR. *Solid State Nucl. Magn. Reson.* **2004**, *26* (1), 11–15.